

4.3 Validity and Scalability of Flow Rate Characteristics

Since flow is a boundary-value problem, the complete conditions to be examined for similarity are (1) governing equations of flow, (2) boundary conditions, and (3) initial values of flow. If phase change such as cavitation occurs in the flow, it must be considered in the governing equations. Based on the similarity, we can discuss the scalability of the flow rate characteristics.

4.3.1 Governing Equations

The governing equations of flow in the flow damper are the equation of continuity and the Navier-Stokes equation for incompressible flow without cavitation. The dimensionless forms of these equations and the boundary conditions of the flow damper give two dimensionless numbers: a Reynolds number for internal flow and a Froude number for a free surface. Strouhal number and Euler number are implicitly used to convert experimental data to the values of the full scale flow damper and are not necessary to be considered here. Therefore, a Reynolds number will affect the resistance of the internal flow in the flow damper without cavitation, while a Froude number will affect the behavior of the free surfaces in the accumulator tank and the standpipe. The fluid properties such as density and viscosity affect flow only through these dimensionless numbers.

Since cavitation bubbles may reduce the flow rate, a cavitation parameter is another parameter that affects the flow resistance of the flow damper in addition to the Reynolds number. Generally speaking, friction coefficients become constant as the Reynolds number gets larger. If the effect of friction can be neglected at a large Reynolds number, a cavitation parameter will be the only parameter of the flow rate coefficient.

Table 4.3-1 shows the Reynolds numbers for the 1/5-scale model, the full height 1/2-scale model and the actual plant. This table shows that each Reynolds number is generally large enough that the effect of friction can be neglected.

Table 4.3-1 Comparison of Reynolds number

	Reynolds Number
Actual Plant	()
Full height 1/2-scale model	
1/5-scale model	

Note: Reynolds numbers are calculated with respect to the throat.

4.3.2 Boundary Conditions

The boundary conditions are (1) boundary configuration, (2) inlet condition, and (3) outlet condition.

Since the 1/2-scale model is completely similar geometrically to the full scale flow damper,

the similarity of the boundary configuration is thoroughly satisfied. Water level in the accumulator tank behaves in a one dimensional manner, and the full heights of the test tank and the standpipe do not affect the flow rate characteristics of the flow damper. The tank pressure of the full-height 1/2-scale tests was identical to the actual pressure of the plant, so the inlet condition is satisfied. The heights of the test tank and the standpipe were full height and the other dimensions were 1/2 scale. The reason of the full height was to simulate the one-dimensional behaviors of the water levels in the test tank and the stand pipe under the actual pressure. The pressure in the exhaust tank was set at the pressure which was determined based on the postulated accident. The outlet condition is, thus, satisfied. Flow rate was determined by the results of the experiments.

Consequently, the boundary conditions were satisfied for similarity.

In addition, the similarity of the 1/5-scale tests under low pressure conditions was also satisfied based on the similar configurations and dimensionless variables.

4.3.3 Initial Conditions

The water in the accumulator tank is stationary at the start of injection. This is also true for the 1/2- and 1/5-scale tests. Therefore, the initial conditions are satisfied.

4.3.4 Scalability of Flow Rate Characteristics

As discussed above, the complete conditions for similarity of the flow rate characteristics of the flow damper are satisfied with the 1/2-scale tests. Then, we can evaluate whether or not viscosity is a significant factor for the flow rate characteristics of the flow damper, using the data of the 1/2- and 1/5-scale tests.

Viscosity would affect the 1/5-scale tests more than the 1/2-scale tests and the full scale flow damper because the Reynolds number is smaller for the 1/5-scale model than the others.

Therefore, if the difference of the flow rate characteristics between the 1/5- and 1/2-scale models is negligibly small, we can deduce that the difference of the flow rate characteristics between the 1/2-scale model and the full scale flow damper is also negligibly small.

Fig.4.3-1 shows the flow rate coefficient with respect to cavitation parameters obtained by the 1/5-scale and full height 1/2-scale models of the flow damper. There are two lines: one for the large flow rate injection and the other for the small flow rate injection. The data for both 1/5-scale and full height 1/2-scale models collapsed into the same lines for large and small flow rates. There is a small discrepancy in the data at a cavitation parameter equal to about 1 to 2 for large flow injection. The difference in Reynolds number would cause the flow rate coefficient of the 1/5-scale tests to be smaller than that of the 1/2-scale tests. Therefore, the discrepancy in the test data shown in Fig.4.3-1 is not attributable to the difference in Reynolds number. The discrepancy is ascribed to the error of the 1/5-scale tests.

Fig. 4.3-1 Flow Rate Coefficient with Respect to Cavitation Factor of the Flow Damper for Full Height 1/2 Scale and 1/5 Scale Models

Consequently, the flow rate characteristics with respect to cavitation parameter shown in Fig. 4.3-1 are the flow characteristics applicable to the actual ACC.

The trend that the flow rate coefficient lessens as the cavitation parameter gets smaller for the large flow rate injection is reasonable, because cavitation is stronger for a smaller cavitation parameter. The flow rate coefficient approaches a constant value as the cavitation parameter gets larger because cavitation is reduced and vanishes for larger cavitation parameters.

Since there is no cavitation at the throat for the small flow rate injection, the flow rate coefficient for small flow should be independent of a cavitation parameter as shown in Fig. 4.3-1.

In the case of the full height 1/2 scale model, an accumulator tank with the same height and the same nitrogen-gas pressure as that of the actual ACC gives the same Froude number as that of the actual ACC for a given backpressure (i.e., RCS pressure). It simulates the same transients of injection velocity, water level in the standpipe, and pressures in the test apparatus as those of the actual ACC. We can thus confirm the injection of cooling water at the actual conditions with that of the full height 1/2 scale model.

The results of the computational fluid dynamics (CFD) support the conclusion mentioned above that there is no significant discrepancy between the flow rate characteristics of the 1/2-scale and the full scale dampers. (Ref. 4.3-1)

The performance of the actual accumulator will be confirmed in a pre-operational test.

4.3.5 Geometrical Parameters for the Performance

S. S. Fineblum reported his excellent experimental results on various geometries of vortex diodes in 1974 (Ref. 4.3-2). Inverse flow in vortex diodes is similar to flow in the vortex chamber of the flow damper for small flow injection. His paper is useful to investigate the effects of the geometrical parameters of vortex chambers on the performance of the flow diode for small flow injection.

J. W. Stairmand proposed the boundary layer coefficient, BLC^* , as an index to evaluate the effect of viscosity on circulation in a vortex chamber. J. W. Stairmand found that, when BLC^* is 0.25 or less, the flow within the vortex chamber conserves circulation. (Ref. 4.3-3)

Using these two references, the geometrical parameters were examined estimate their effect on the performance of the flow damper for small flow injection. The conclusion is that the significant parameters were the ratios of the diameters of the vortex chamber to its outlet port and the height to the diameter of the chamber. These parameters were fully similar to the 1/2-scale and full scale vortex dampers as shown in Appendix A.

4.3.6 Index of Cavitation

Cavitation may occur for large flow injection, but will not occur for small flow injection. A cavitation parameter is a dominant index of inception and strength of cavitation. When cavitation inception occurs, a cavitation parameter is equivalent to the negative pressure coefficient with the critical pressure as its minimum pressure. After inception the value decreases, and the cavitation parameter assumes a definite value at each stage of development or "degree" of cavitation on a particular body (Ref. 4.3-4). A cavitation parameter, therefore, can be used for both the 1/2-scale and full scale flow dampers, because the pressure coefficient is common for similar bodies.

4.3.7 Effect of Nitrogen

A 1/2-scale test was performed with saturation of dissolved nitrogen. In this test case, large numbers of tiny bubbles equal to about 1 mm in diameter were observed and rose to the surface in the test tank just after the start of the injection. These bubbles reduced the superficial density of fluid and resulted in a 2-sec delay in completing large flow injection. Since the pressure of the 1/2-scale tests was identical to that of the full scale accumulator, this behavior of nitrogen in the model tank is the same as that in the actual accumulator tank.

4.4 Quality Assurance of the ACC Test Program

1) General

The results of the ACC test program, performed from June 1994 to August 1996, are applicable to the US-APWR. These results were reviewed and MHI confirmed that the requirements of the Japanese QA Guideline and QA activities at that time met the requirements of 10 CFR 50 Appendix B and ASME NQA-1-1994, by comparing the requirements of the Japanese QA Guideline to those of 10 CFR 50 Appendix B and ASME NQA-1-1994.

2) Procedure of Re-verification

The ACC test program was re-verified and confirmed to be reliable and accurate for use in the US-APWR. This re-verification was performed by evaluating the following items in accordance with a written procedure.

- (1) Confirmation of Test Procedure
- (2) Evaluation of Test Personnel
- (3) Evaluation of Test Equipment
- (4) Evaluation of Test Procedure (execution)
- (5) Evaluation of Test Results
- (6) Evaluation of Design Personnel Concerning to the Test

3) Results

It was confirmed that the reliability and accuracy for the ACC test program satisfied the requirements of 10 CFR 50 Appendix B and ASME NQA-1-1994.

The following sets out the re-verification results of the above six items.

(1) Confirmation of Test Procedure

The ACC test program can be applied to the US-APWR by comparing the test conditions as follows:

- MHI established test conditions for the ACC of the US-APWR consistent with the design requirements for the ACC of the US-APWR.
- MHI compared the previous APWR test conditions with the test conditions established for the US-APWR and confirmed that the previous test conditions are applicable to the US-APWR.
- The test conditions that were compared and confirmed were the following prerequisite conditions for the test:
- Prerequisites: - Adverse conditions (considering operating modes and environments)
 - Configuration
 - Test scope addressed applicable design features

(2) Evaluation of Test Personnel

It was confirmed that the test personnel who had conducted the previous tests satisfied the current necessary qualifications as follows:

- MHI reviewed the qualifications of the test personnel who had conducted the previous tests against current qualification requirements (NQA-1-1994 2S-1).
- MHI established records documenting this re-verification of the qualifications of the testing personnel.

(3) Evaluation of Test Equipment

It was confirmed that the condition and the accuracy of the test equipment and measurements used during the testing met current requirements taking into account the test objectives for the US-APWR. The results of this validation were as follows:

- MHI documented the test objectives and test results required for the US-APWR based on the design conditions for the ACC of the APWR.
- Based on this document, MHI established the requirements for the accuracy of test equipment and measurements for the US-APWR.
- MHI determined that the accuracy of the test equipment and measurements used in the ACC test program at that time satisfied the requirements for the US-APWR.

(4) Evaluation of Test Procedure (execution)

It was confirmed that the test procedure used for conducting the ACC tests at that time meets the current requirements as follows:

- MHI documented the design requirements for the US-APWR (i.e., items that must be verified in the test) based on the design conditions for the ACC as used in the US-APWR.
- MHI confirmed that the test procedure used at that time the tests were conducted meets the present requirements and are appropriate by comparing the items that were to be verified by those tests with the above identified design requirements for the US-APWR to be verified by test.

(5) Evaluation of Test Results

Test results were evaluated by the responsible design organization and it was confirmed that the test results obtained could be applied to the US-APWR.

- MHI documented this evaluation of the applicability of the past test results to the US-APWR.

(6) Evaluation of Design Personnel Concerning to the Test

Design personnel responsible for the test at that time had participated in the test process from the commencement of test preparations (e.g. test plan, test procedure, test equipments) to the completion of the tests and had both witnessed and evaluated the test results. MHI also confirmed that design test program was independently reviewed by experienced engineers and the tests were witnessed by representatives of the funding the design personnel of utilities and MHI. Therefore, the test at that time was objective. MHI confirmed that the design personnel had participated in the design of the test plan, test procedure, and test equipment and also in the evaluation of test results from evidence such as meeting minutes, trip reports and document review reports etc.

- MHI confirmed based on meeting minutes, trip reports, etc. that meetings concerning the test plan, test procedure, and test equipment had been held with the utilities and that the designs had been reviewed by the utilities and their comments had been incorporated.
- MHI confirmed that the design personnel of utilities and MHI had witnessed the actual test.
- MHI confirmed that the design review (e.g. Design Review Board) for the overall review of the test, including the test plan, test procedure, test equipment, and test results, was conducted by independent experienced engineers.

5.0 CONCEPT OF THE SAFETY ANALYSIS MODEL

5.1 Characteristic Equations of Flow Rates for the Safety Analysis

The flow rate coefficient is a function of the cavitation factor as shown in Fig.5.1-1. Experimental formulae of the flow rate characteristics of the flow damper were derived with respect to a cavitation factor separately for the large and small flow rate injections each by curve fitting using the data of the full height 1/2-scale tests. The curve fitting is based on the least-squares method. An exponential function was chosen as the form of the fitting curves to give the best fitting of the data. The resultant experimental equations are:

$$C_v = 0.7787 - 0.6889 \exp(-0.5238\sigma_v) \text{ For Large Flow Rate Injection,} \quad (5-1)$$

and

$$C_v = 0.07197 - 0.01904 \exp(-6.818\sigma_v) \text{ For Small Flow Rate Injection} \quad (5-2)$$

The flow resistance coefficient of the flow damper (K_D) is given by

$$K_D = \frac{I}{C_v^2} \quad (5-3)$$



Fig. 5.1-1 The Flow Characteristics of the Flow Damper

5.2 Estimation of Uncertainty of the Characteristic Equations of Flow Rates

The data from the full-height, full pressure, 1/2 diameter experiment was used to develop the characteristic equations for the ACC performance. Errors of measured values consist of experimental errors, instrument errors and manufacturing errors. The causes of experiment errors may be turbulence, unsteadiness of flow, structural vibration, noises, etc. The causes of instrument errors may be sensitivities of sensors, linearity of instruments, etc. The causes of manufacturing errors may come from machining and assembling accuracies.

The total error of a measured value was, however, divided into a bias error and a random error according to ANSI/ASME PTC19.1-1985 as described below. In LOCA analysis, uncertainty of characteristic equation will be considered conservatively to evaluate fuel cladding temperature using these errors.

Random Errors

Pressures and water levels were measured as a function of time. The raw data generally scatter and form a band with time. For LOCA analysis, it is necessary to use the reduced data without dispersion that represent the flow rate characteristics of the flow damper. These reduced data were taken by curve fitting of the raw data to make a curve that lies at the middle of the data band. The experimental equations were derived from the curves. The standard deviation of the dispersion of the data from the experimental equations was evaluated as random errors for each test case as shown in Table 5.2-1.

Table 5.2-1 Dispersion of the Data from the Experimental Equations



Instrument Uncertainties

A true value may be different from the experimental equations. This difference is defined as an experimental error. However, the true value is not known and needs to be estimated. Each string of a sensor, an amplifier, an A/D converter and a process computer was calibrated one by one. Instrument uncertainties consist of accuracy of each instrument string as a bias error and sampling error of each calibration as a random error and were calculated by root-sum-square of them. Instrument uncertainties associated with flow rate coefficients is shown for each test case in Table 5.2-2.

Table 5.2-2(1/2) Instrument Uncertainties at Large Flow



Table 5.2-2(2/2) Instrument Uncertainties at Small Flow



Manufacturing Errors

The manufacturing error of the flow damper associated with the flow rate coefficient is determined based on the dimensions and manufacturing tolerance of the following parts that affect the performance of the flow damper.

- The inner diameter of the throat
- The facing angle (collision angle) of the large flow inlet pipe and the small flow inlet pipe
- The inner diameter of the vortex chamber
- The width of the small flow pipe
- The height of the small flow pipe

Consequently, the manufacturing error associated with the flow rate coefficient will be less than{ }.

5.3 Estimation of Potential Uncertainties of Water Level for Switching Flow Rates

The uncertainty in the switching levels as function of the water level in the test tank was taken from elevation data of the inlet port of standpipe in full height, full pressure, 1/2 diameter experiments. A water level at switching of flow rates was defined as an intersecting point of two curves of water levels for large flow rate injection and small flow rate injection. The instrument errors were also counted in the estimation of the uncertainties.

Uncertainty of water level for switching flow rates in each test case is shown in Table 5.3-1.

Table 5.3-1 Uncertainty of Water Level for Switching Flow Rates



5.4 LOCA Analytical Model and Computational Procedure

The resistance coefficient of the flow damper varies over time depending on the flow condition. The resistance coefficient is calculated by the correlation equations between cavitation factor and flow rate coefficient.

The correlation equations are incorporated into the LOCA analysis computer code and resistance coefficient of the flow damper is calculated at each time-step in the LOCA analysis. Compared with the ACC, the resistance coefficient of a conventional nuclear plant accumulator does not vary for conditions such as pressure and flow rate.

The computational procedure for determining the resistance coefficient of the ACC is determined as follows;

- 1) Calculate cavitation factor σ_v from the flow condition at the flow damper.

$$\sigma_v = \frac{P_D + P_{at} - P_v}{(P_A + \rho g H) - \left(P_D + \frac{\rho V_D^2}{2} + \rho g H' \right)} \quad (5-4)$$

Where,

σ_v	:	Cavitation factor
P_{at}	:	Atmospheric pressure
P_D	:	Flow damper outlet pressure [gage]
P_A	:	Gas pressure in accumulator
P_v	:	Vapor pressure
ρ	:	Density of water
g	:	Acceleration of gravity
H	:	Distance between ACC water level and vortex chamber
H'	:	Distance between outlet pipe and vortex chamber
V_D	:	Velocity of injection pipe

- 2) Calculate the flow rate coefficient C_v using the following correlations.

$$\text{For large flow rate:} \quad C_v = 0.7787 - 0.6889 \exp(-0.5238 \sigma_v) \quad (5-5)$$

$$\text{For small flow rate:} \quad C_v = 0.07197 - 0.01904 \exp(-6.818 \sigma_v) \quad (5-6)$$

The injection flow rate switches to small flow rate when the calculated accumulator water volume becomes less than the volume below the standpipe inlet level.

Uncertainty of characteristics equations is considered conservatively to evaluate fuel cladding temperature in LOCA analysis.

- 3) Convert flow rate coefficient C_v to resistance coefficient of the flow damper K_D .

$$K_D = \frac{I}{C_v^2} \quad (5-7)$$

- 4) Calculate total resistance coefficient by summing up resistance coefficient of the flow damper and that of injection piping.

$$K_{acc} = K_D + K_{pipe} \quad (5-8)$$

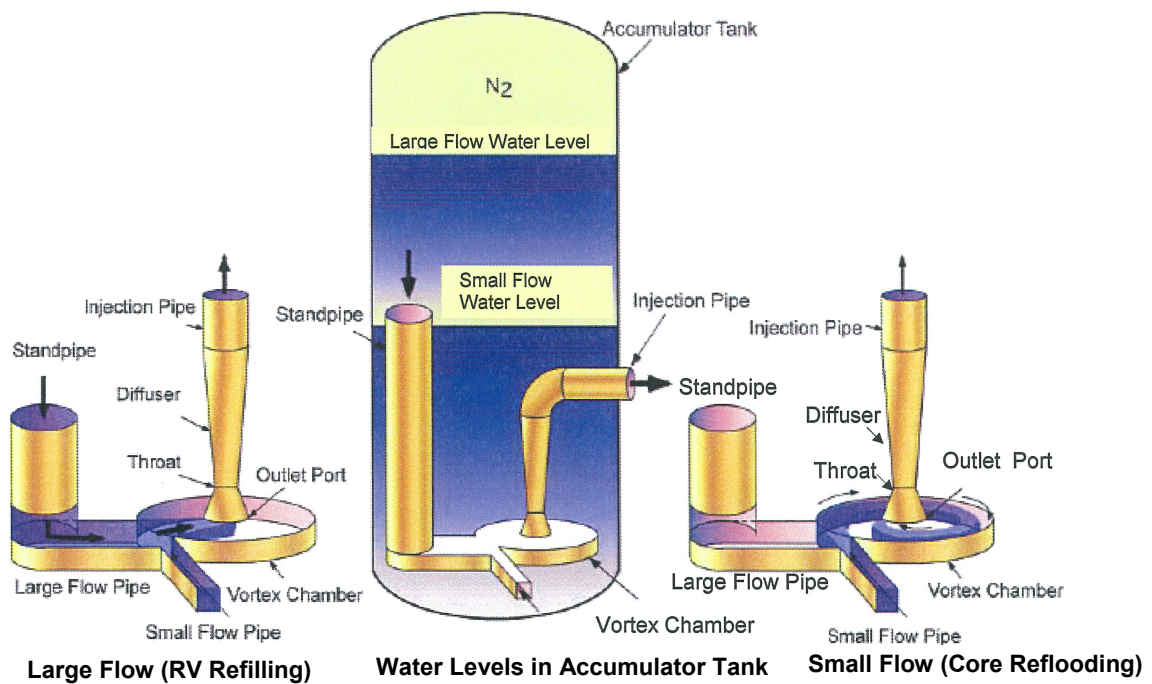
Where,

K_{acc} : Total resistance coefficient of the flow damper and injection piping
 K_{pipe} : Total resistance coefficient of injection piping

6.0 SUMMARY

The Mitsubishi Heavy Industries, Ltd. Advanced Accumulator (ACC) design will be used in MHI's Advanced Pressurized Water Reactors. The ACC design simplifies the emergency core cooling system design by integrating the short term large flow rate design requirements currently satisfied in conventional pressurized water reactor designs by the combined injection capabilities of the primary system accumulator and the low head safety injection pump into a single passive device, the ACC.

The ACC is a borated water storage tank with a fluidic device that throttles the flow rate of cooling water injected into a reactor vessel from a large to a small flow rate. A conceptual drawing of the ACC is shown below.



The vortex chamber at the inlet of the injection pipe in the accumulator tank accomplishes the flow rate throttling from large flow to small flow by establishing a vortex (and thus a large pressure drop) at a predetermined accumulator tank level. The inlet of the standpipe is located at the ACC volume level at which the transition from large to small flow is desired to occur. The ACC is a simple device that achieves precise throttling from a large injection flow rate to a small injection flow rate with no moving parts.

Upon initiation of a large break loss of coolant accident, all short term low head primary coolant injection flow requirements are satisfied by the ACC. Following depletion of the ACC water volume, the longer term ECCS flow requirements are met by the safety injection pumps thus eliminating the need for low head injection pumps. The immediate availability of low head flow provided by the ACC upon loss of electrical power coincident with a large break loss of coolant accident provides additional time for actuation of the backup emergency power source.

The design requirements and specifications of the ACC for the US-APWR are the same as that for the APWR. The confirmatory test program for the APWR was successfully conducted as a joint study among five utilities (Japan Atomic Power Co., Hokkaido Electric Power Co., Kansai Electric Power Co., Shikoku Electric Power Co., and Kyushu Electric Power Company) and MHI, from September 1994 to September 1996. The tests confirmed the principles of operation of the flow damper and successfully established the ACC flow characteristics. Specifically, the testing confirmed that:

1. No vortex was formed during large flow and a stable vortex was formed during low flow in the vortex chamber
2. Sharp flow rate switching occurred without gas entrainment.
3. The flow characteristics of the flow damper were organized by dimensionless numbers and were independent with scaling.

Empirical flow rate coefficients have been developed from the test results and will be used in an integrated thermal hydraulic model of the US-APWR Reactor Coolant and ECCS systems to assure the US-APWR meets or exceeds all US safety standards.

The ACC design is expected to improve the safety of pressurized water reactors by the innovative application of the flow damper to assure the early stage of LOCA injection flow is satisfied by an inherently reliable passive system. This innovation reduces the necessity of relying on maintenance sensitive components such as low head safety injection pumps for assuring LOCA injection flow, provides additional time for actuation of backup emergency power for loss of power coincident with a large break LOCA, and reduces the net maintenance and testing burden by the elimination of low head safety injection pumps from the LOCA mitigation strategy.

7.0 REFERENCES

- 4.3-1 CFD Analysis for Advanced Accumulator, MUAP-09025-P Rev. 1 (Proprietary), and MUAP-09025-NP Rev. 1 (Non-Proprietary), March 2011.
- 4.3-2 S.S. Fineblum: Vortex Diodes, pp. 48-80, Proceedings of the Fluidic State-of-the-art Symposium Held at Naval Ordnance Laboratory, White Oak, Maryland on 30 September - 3 October, 1974.
- 4.3-3 J. W. Stairmand: Flow patterns in vortex chambers for nuclear duties, Vol. 29, No. 6, pp. 413-418, Nucl. Energy, Dec., 1990
- 4.3-4 R. T. Knapp, et. al, Cavitation, p. 43, McGraw-Hill, 1970.

Geometrical Parameters for the Performance

S. S. Fineblum reported his excellent experimental results on various geometries of vortex diodes in 1974 (Ref. 4.3-2). Inverse flow in vortex diodes is similar to flow in the vortex chamber of the flow damper for small flow injection. His paper is useful to investigate the effects of the geometrical parameters of vortex chambers on the performance of the flow diode for small flow injection. Here is the summary of his report.

1) Experiments

The vortex chambers used in his experiments varied in diameter, D , from 1.58 to 3.25 inches (40 to 82.6 mm) and in length, L , (equivalent to height of the vortex chamber, H) from 0.188 to 1.0 inches (4.78 to 25.4 mm). The nozzles varied in width from 0.016 to 0.4275 inches (0.4 to 11.1 mm), and the outlet varied in diameter from 0.179 to 0.394 inches (4.6 to 10.0 mm). The maximum available pressure, p , and flow, Q , were 100 psi (6.90×10^5 N/m²) and 6 gpm (3.79×10^{-4} m³/sec). It is not clearly mentioned in the paper, but gas or air seemed to be used as the working fluid, because of the large tangential velocities of the diodes. If the working fluid was air at 305 K in temperature, the maximum dimensionless flow rate (equivalent to Reynolds number) $q^* = Q/(2\pi H\nu)$, is from 82 to 440. ν is the kinematic viscosity of the fluid.

The flow damper of the 1/2-scale model was [] mm in diameter and [] mm in height (equivalent to his length), respectively. The maximum pressure was 758 psi gauge (5.23MPa gauge). The maximum flow rate was about [] for large flow injection and about [] for small flow injection. The working fluid was city water. The actual flow damper is double in size, 4 times in flow rate, and same in pressure as the 1/2-scale damper. The dimensionless flow rate, q^* , is [] for the 1/2-scale damper and [] for the full-scale damper at 305 K in temperature. Since the dimensionless flow rate, q^* , of the 1/2-scale model is two order larger than that of the vortex diodes, viscosity less affects the performance of the flow damper than that of the vortex diodes in Fineblum's study.

2) Vortex Pressure Drop Coefficient

The pressure drop coefficient K is defined as:

$$K = \frac{P_o - P_i}{\frac{\rho}{2} V_N^2} = \frac{1}{n} (1 - R^{2n}) \quad (1)$$

where R is the ratio of the outer-to-inner radii of vortex diodes, $R=r_i/r_o$, r_i the radius of the vortex chamber, r_o the radius of the outlet port, and n the vortex exponent. The exponent, n , varies between -1 (forced vortex) and 1 (free vortex).

The tangential velocity, V , at an arbitral radius, r , is assumed to have the form of:

$$V \equiv V_N \left(\frac{r_i}{r} \right)^n, \quad (2)$$

where V_N is the tangential velocity from the nozzle.

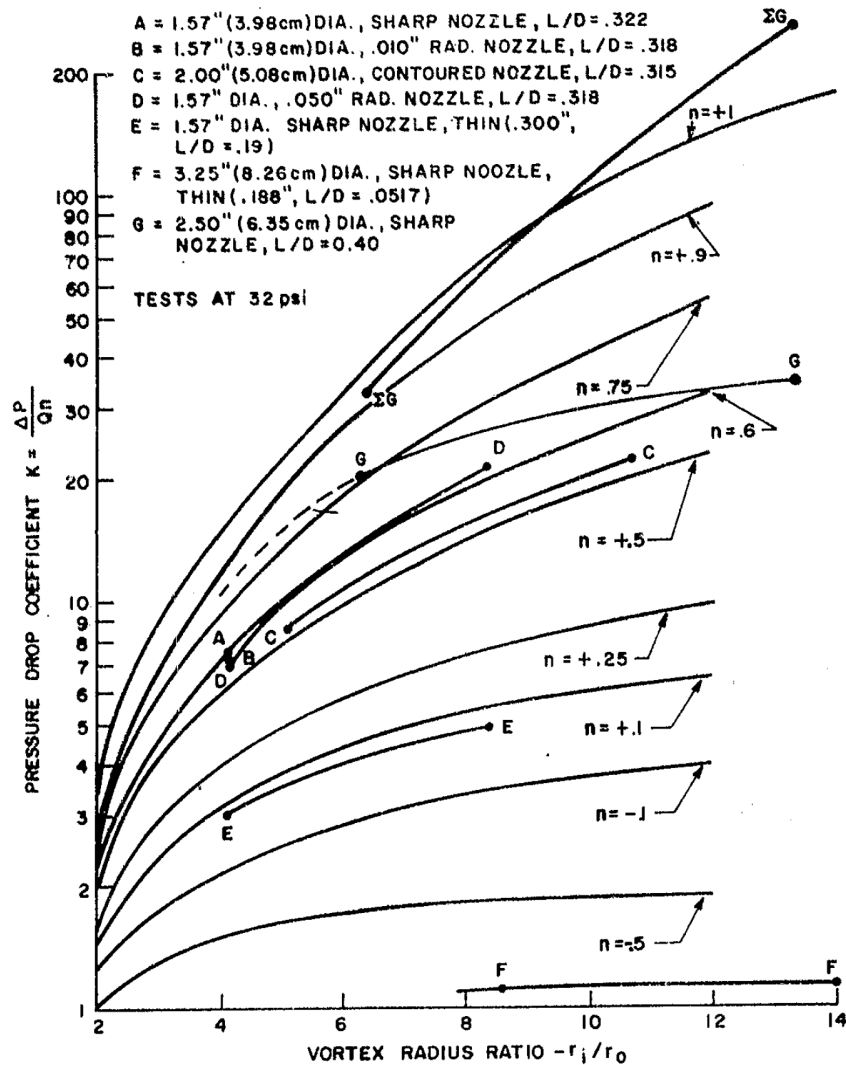


Fig. 1 Test Results: Total Pressure Drop Coefficient across Diode Versus Radius Ratio (from S. S. Fineblum)

The variation of the pressure drop coefficient, K , with respect to the ratio of radii, R , is shown in Fig. 1. Lines of computed K versus R with constant values n are plotted for comparison. The results of Fineblum show that for most vortex chambers the effective vortex exponent is approximately constant. The vortex exponent, n , should be chosen as an effective n to express the fact that many modes of flow in the vortex chamber result in a specific pressure drop and that the resulting pressure drop coefficient is a function of R . Therefore, n is an average correlation quantity rather than a true vortex exponent indicating the exact mode of vortex flow. The real flow in the vortex chamber is three dimensional due to the growth of boundary layers on the walls, which cannot be expressed by Eq. (2). Therefore, the vortex exponent " n " cannot be theoretically determined, but has to be experimentally determined.

3) Boundary Layer Coefficients

The boundary layer coefficient, BLC^* , is an index to evaluate the effect of viscosity on circulation in a vortex chamber. J. W. Stairmand found that, when BLC^* is 0.25 or less, the flow within the vortex chamber conserves circulation (Ref. 4.3-3). In other words, viscosity has little effect for this BLC^* . If BLC^* is between 0.25 and 0.5, viscosity has a slight effect. And, if BLC^* is 4.0 or larger, the flow in the vortex chamber does not conserve circulation at all. It is clear that most of the Fineblum's vortex diode test results were strongly affected by viscosity, as discussed below.

Fig. 2 shows BLC^* with respect to the dimensionless flow rate, q/v . BLC^* s of the vortex diodes are calculated based on the data in Fig. 4.3-2 and the sizes of the vortex diodes are 0.42 for Type G, 2.7 for Type A, 2.8 for Types D and B, 5.5 for Type C, 7.8 for Type E and 55 for Type F. The diodes in order from largest to smallest vortex exponent are Types G, A, D, B, C E and F. It is clear that the performance of the tested vortex diodes was dominantly affected by viscosity. The blue squares indicate BLC^* s of the vortex diodes and the red circles indicate those of the advanced accumulator flow dampers. The BLC^* s of the vortex diodes are on a line except Type C which has large swirl numbers, $S=w_i/v_i$, where w_i and v_i are the tangential and centripetal radial velocities, respectively.

BLC^* s of the flow dampers are much larger in dimensionless flow rate than those of the vortex diodes. The BLC^* s of the 1/2- and 1/1-scale dampers were 0.337 and 0.283, respectively. Viscosity, then, has a minor effect for the flow in the flow damper contrary to the vortex diodes. Therefore, the test results by Fineblum are still very useful to qualitatively investigate the flow in the vortex chamber of the flow damper, but it is necessary to consider the different impact of viscosity effects when applying Fineblum's results to the advanced accumulator.



Fig. 2 BLC^* with respect to Dimensionless Flow Rate

4) Height-to-Diameter Ratio

For very thin diodes the boundary layers on its disk walls will completely fill the chamber. As the height increases, the available distance free of the boundary layers increases. Once this free distance is much greater than the boundary layer, further increase in L/D is not beneficial.

The average vortex exponent, n , increases with L/D as seen in Fig.3. It supports the fact mentioned above. In the cases of the vortex diodes, the vortex exponent, n , becomes relatively insensitive to any increase above L/D=0.35. The insensitive limit must depend on viscosity. If viscosity effect is smaller, thickness of the boundary layer on the wall in the vortex chamber must be thinner to give smaller insensitive limit of L/D. L/D for the flow damper of the advanced accumulator is [] and smaller than 0.35. But the vortex exponent n of the advanced accumulator seems to be large per the following discussion.

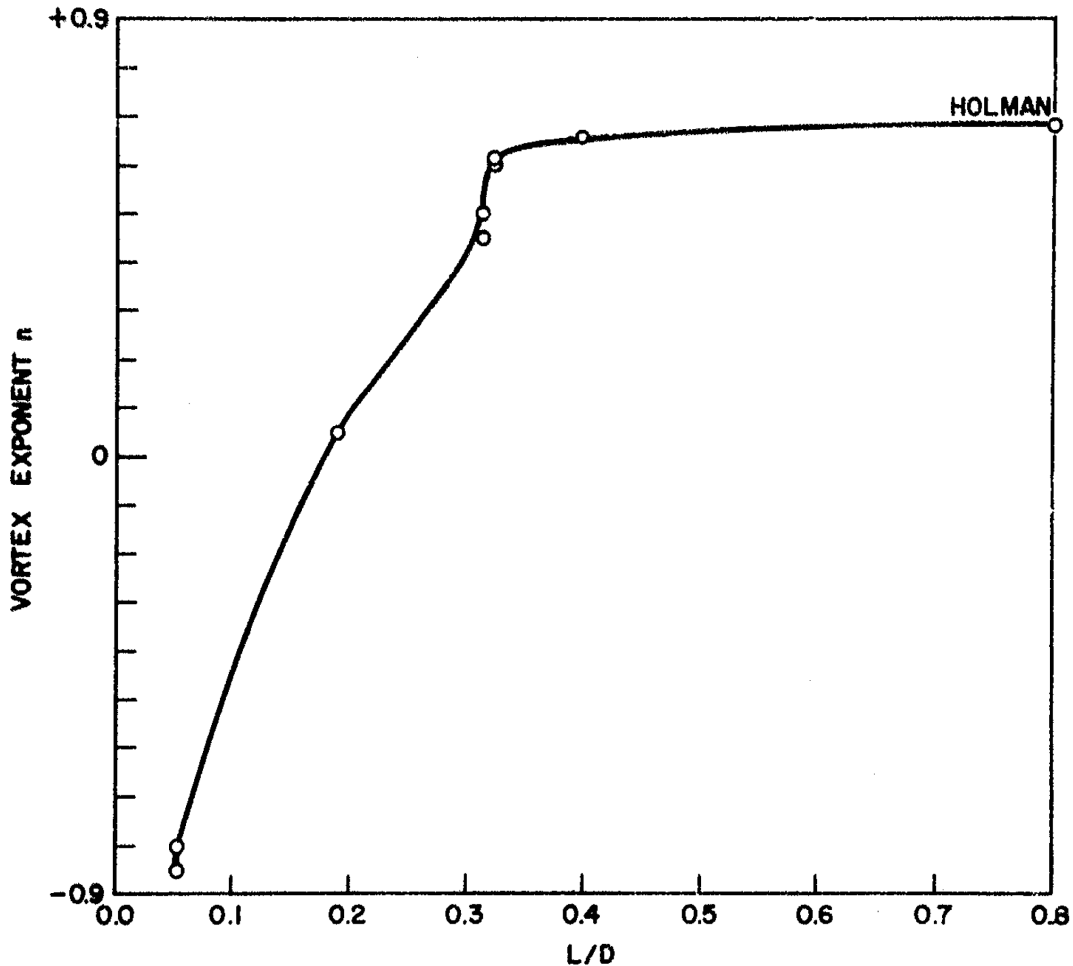


Fig. 3 Variation of Vortex Exponent, n , with respect to Ratio of Vortex Height to Diameter (from S. S. Fineblum)

Fig. 4 shows the vortex exponent, n , with respect to BLC^* calculated based on the data in Fig. 1. The blue squares indicate BLC^* 's of the vortex diodes and the red circles indicate

those of the flow dampers. The BLC^* s of the vortex diodes are on a straight line except Type E that has a thin vortex chamber. Type F also has a thin vortex chamber and small vortex exponent, $n=-0.85$. The line approximating the data of the vortex diodes (except Type E) is also shown in the figure.

If it is assumed that the flow damper is also on the line, the red circles are the design points of the 1/2- and full scale dampers. Consequently, the small difference in BLC^* s of the 1/2 to 1/1 advanced accumulators is expected to have a negligible effect on vortex exponent.



Fig. 4 Vortex Exponent, n , with respect to BLC^*

5) Vortex Chamber Outlet

Fineblum and some other authors addressed that the flow field in a vortex chamber is primarily "a strong two-dimensional vortex superimposed on a weak sink" and the exact shape of the vortex chamber outlet is not important.

This is also true of the flow damper for small flow injection. But we have to be careful not to make any additional pressure loss at the chamber outlet for large flow injection. This is the reason that we select a reducer just after the chamber outlet of the flow damper.

6) Vortex Generated Pressure Drop in Outlet Tube

Fineblum stated that, "In most cases, the pressure drop measured across the outlet tube was relatively insignificant. However, at very high values of vortex radius ratio and vortex pressure drop coefficient, the pressure drop through the outlet tube is a major portion of the total." In this case, the pressure drop in the tube immediately downstream of the vortex chamber contributes significantly to the vortex generated pressure drop. This fact agrees with the calculated results of the flow damper by CFD (Ref. 4.3-1).

We have to pay attention to the fact that the swirl flow in the outlet tube originates in the vortex chamber. This means that the pressure loss by swirl flow in the outlet tube is controlled by the vortex in the vortex chamber. Strictly speaking, the dynamic pressure converted from static pressure in the vortex chamber is lost in the outlet tube, if there is no static pressure recovery. [

.]

7) Pressure Drop Through the Tangential Nozzle

Fineblum has discussed the pressure drop through the tangential nozzle only for forward flow, but not for inverse flow. That is because the inverse flow does not cause flow separation in the tangential nozzle to induce a strong vortex in the vortex chamber. [

]

For the advanced accumulator, the initial velocity distribution should be the same since the geometry of the large and small flow pipes and the collision angle is the same.

8) Conclusions

The geometrical parameters were examined for the performance of the flow damper, using the references by S. S. Fineblum and J. W. Stairmand. As a result, the 1/2-scale and full scale flow dampers are ascertained to be in a good configuration which reduces the influence of viscosity and attains consistent performance between scales.